J Mater Sci

Energy materials

Low-temperature fabrication of morphology-controllable Cu_2O for electrochemical CO_2 reduction

Rabin Dahal[1], Schindra Kumar Ray[1,*], Gayani Pathiraja[2], and Bishnu Prasad Bastakoti[1,*]

[1] *Department of Chemistry, North Carolina A and T State University, 1601 E Market St, Greensboro, NC 27411, USA*
[2] *Department of Nanoscience, Joint School of Nanoscience and Nanoengineering, University of North Carolina at Greensboro, Greensboro, NC 27401, USA*

Received: 18 May 2024
Accepted: 11 July 2024

ABSTRACT

Cu_2O has been successfully synthesized in different morphologies/sizes (nanoparticles and octahedrons) via a low-temperature chemical reduction method. Trapping metal ions in an ice cube and letting them slowly melt in a reducing agent solution is the simplest way to control the nanostructure. Enhancement of charge transfer and transportation of ions by Cu_2O nanoparticles was shown by cyclic voltammetry and electrochemical impedance spectroscopy measurements. In addition, nanoparticles exhibited higher current densities, the lowest onset potential, and the Tafel slope than others. The Cu_2O electrocatalyst (nanoparticles) demonstrated the Faraday efficiencies (FEs) of CO, CH_4, and C_2H_6 up to 11.90, 76.61, and 1.87%, respectively, at −0.30 V versus reference hydrogen electrode, which was relatively higher FEs than other morphologies/sizes. It is mainly attributed to nano-sized, more active sites and oxygen vacancy. In addition, it demonstrated stability over 11 h without any decay of current density. The mechanism related to morphology tuning and electrochemical CO_2 reduction reaction was explained. This work provides a possible way to fabricate the different morphologies/sizes of Cu_2O at low-temperature chemical reduction methods for obtaining the CO, CH_4, and C_2H_6 products from CO_2

Introduction

The world's energy consumption is extremely dependent upon fossil fuels, which causes energy shortages and environmental problem issues via CO_2 gas emission [1–5]. Researchers focus on capturing, storing, and converting CO_2 to solve these issues. Among them, CO_2 conversion is the most prominent route because it can transmute CO_2 into fuels and useful chemicals [6]. The electrochemical CO_2 reduction reaction (CO_2RR) is one of the most promising strategies in CO_2 conversion technique because of green technology and

Handling Editor: Naiqin Zhao.

Address correspondence to E-mail: schindrakumarray@gmail.com; bpbastakoti@ncat.edu

https://doi.org/10.1007/s10853-024-10004-z
Published online: 25 July 2024

controllable reduction potential/reaction temperature under ambient conditions [7]. Recently, Cu-based electrocatalysts have been widely applied for CO_2RR because of several advantages such as low cost, intermediate binding energy for adsorbed CO (*CO), high yield of multi-carbon products, low overpotential, different oxidation states, non-toxic, competing hydrogen evolution reaction, and their stability [8, 9].

Copper oxide (Cu_2O) is considered a superior electrocatalyst for CO_2RR among Cu-based materials because of its ability to trap the subsurface oxygen, kinetically favorable, enhancement of *CO binding, and higher C1/C2 selectivity [10]. Various strategies (facet, defect, morphology, and heterostructure) have been applied to enhance the electrochemical CO_2RR performances. Among these strategies, morphology-controlled is a perfect way to increase the electrochemical CO_2RR for obtaining C1/C2 products because it can control selectivity and stability [11]. Different synthesis techniques (electrochemical deposition, chemical deposition, chemical reduction, and thermal treatment) have recently been used [12]. However, low-temperature fabrication of morphology-controllable Cu_2O for electrochemical CO_2 reduction has not been reported yet. The low-temperature fabrication technique via ice melting can effectively control the release of reactants, nucleation, and agglomeration of particles in aqueous solution [13]. So, tuning the morphology (shape/size) by low-temperature technique is the perfect option to boost the electrochemical CO_2RR performances of Cu_2O towards producing useful fuels [14].

In the present work, different morphologies/sizes of Cu_2O were synthesized by a simple low-temperature chemical reduction method via ice melting using a strong reducing agent. The variation of precursor concentrations has been applied to control the morphologies/sizes of Cu_2O. The samples were characterized by X-ray diffraction (XRD), field-emission scanning electron microscopy (FESEM), transmission electron microscopy (TEM), and X-ray photoelectron spectroscopy (XPS) measurements. The electrochemical measurements (cyclic voltammetry, electrochemical impedance spectroscopy, linear sweep voltammetry, and chronoamperometry) of samples were obtained by using an H-type cell for electrochemical CO_2RR. Tafel plots, detection of gaseous products, Faradic efficiencies (FEs), and possible mechanism of CO_2RR were explained.

Experimental

Catalyst synthesis

The chemicals used were of analytical grade and were used without further purification. 0.1 mm thickness copper foil was purchased from Merck, Germany. Copper nitrate trihydrate [$Cu(NO_3)_2.3H_2O$] was purchased from Acro's Organic, Poland. Sodium borohydride ($NaBH_4$) was purchased from Spectrum Chemical MFG Corp, California, and ethanol [C_2H_5OH, (95% pure)] was purchased from VWR Chemicals, Canada. The samples were synthesized using a low-temperature chemical reduction method using one-pot synthesis. The main advantage of this method is that it enables the tuning of particles' morphology by slowly releasing Cu ions in the solution because of the slow release of metal ions during the melting of the ice cube compared to other solution-based methods [13]. It was carried out by forming an ice cube of $Cu(NO_3)_2.3H_2O$ solution. $Cu(NO_3)_2.3H_2O$ was weighed and dissolved in 100 mL of distilled water. Different concentrations of $Cu(NO_3)_2.3H_2O$ (0.02 M, 0.1 M, and 0.5 M) were used for the synthesis. During synthesis, the pH of the solution was 4.4. The as-prepared ice cubes were added to $NaBH_4$ solution (0.01 M) in 100 mL ethanol. The sample was collected after 60 min and washed with distilled water and ethanol several times to remove the impurities. The obtained powders were dried and ground using mortar and piston. The catalysts were named Cu_2O-1, Cu_2O-2, and Cu_2O-3 for 0.02 M, 0.1 M, and 0.5 M concentrations of Cu salt, respectively. The schematic illustration of Cu_2O synthesis is shown in Fig. S1.

Material characterization

Powder X-ray diffraction (XRD) patterns were recorded in Rigaku Miniflex 600 (2θ: 10–80°, step: 0.02, and continuous: 1°/min) diffractometer. The morphology of samples was obtained by field emission scanning electron microscopy (FESEM, JEOL, JSM-IT800). Transmission electron microscopy (TEM), high-resolution transmission electron microscopy (HRTEM), and selected area diffraction patterns (SAED) images were recorded by JEOL 2100 PLUS TEM acquired at 120 kV. The X-ray photoelectron spectroscopy (XPS) was carried out on thermo-scientific ESCALAB™ XI (200 eV and Al Kα). Gas chromatography (GC) (SRI 8610C) analyzed the gaseous products.

Electrochemical measurements

The electrochemical measurements were performed in an H-type cell with a three-electrode system. The H-type cell consists of platinum (as a counter electrode), Ag/AgCl electrode (as a reference electrode stored in 3 M KCl solution), and Cu_2O (as a working electrode) in 0.5 M $KHCO_3$ solution. The electrode was prepared by mixing the 0.05 g of sample, and 50 µL Nafion in 500 µL ethanol. The mixture was sonicated for 60 min. The highly dispersed mixture was deposited on the 1 cm × 1 cm copper foil and left to dry for 12 h in an oven at 60 °C. The cyclic voltammetry (CV) of the prepared materials was measured that consists of −0.6 V to 0.6 V potential window with a scan rate between 40 mV/s and 100 mV/s. Similarly, the conductivity of the electrode was studied by electrochemical impedance spectroscopy (EIS) between 0.1 Hz and 100,000 Hz. Likewise, the linear sweep voltammetry (LSV) was studied between 0 and 0.1 V versus the reversible hydrogen electrode (RHE) at the scan rate of 10 mV/s. The following equation was used for the calculation of RHE:

$$E_{RHE} = E_{Ag/AgCl} + 0.197 + 0.059pH \ \left(0.5\text{M KHCO}_3 \sim 8.5\right)$$

where $E_{Ag/AgCl}$ represents the potential against the reference electrode, and 0.197 denotes the standard potential of Ag/AgCl at 25 ºC [15].

A 50 mL H-type electrochemical cell was used. Two compartments (anodic and cathodic) were separated by Nafion 117 membrane. Nafion 117 membrane was used after treatment with 1 M H_2SO_4 and water. The volume of electrolyte used was 35 mL. For the saturation of electrolytes, 99.99% pure CO_2 gas was bubbled in a cathodic cell compartment for 60 min with 10 sccm (standard cubic centimeters per minute) with the help of a mass flow controller (MC-100SCCM-D, Alicat Scientific). The outlet of the cathodic cell compartment was connected to GC. GC was calibrated with a standard gas mixture (ARC3). The gaseous products obtained during the reaction were detected by a flame ionization detector (FID). The current–time (it) measurements were performed at a fixed potential of −0.30 V versus RHE (Supplementary information). Gasses from the cell were injected into GC for 400 s, and electrocatalytic CO_2RR was evaluated. The stability of Cu_2O-1 was performed over 11 h.

Results and discussion

Figure 1 revealed the XRD patterns of catalysts. As observed, the peaks were assigned to cuprite Cu_2O (Pn-3m) along with strong (111) orientation (JCPDS: 05-0667) in all samples [16]. A possible reason for the formation of Cu_2O is associated with the reduction of $Cu(NO_3)_2.3H_2O$ in the presence of a reducing agent and dissolved oxygen under ambient conditions [17, 18]. However, a small peak was observed at 38º (2θ), which suggests the presence of a trace amount of CuO (JCPDS: 45-0937) in Cu_2O-1 [18]. It may be related to Cu(I) oxidation during the synthesis [19]. In addition, a very low intense peak was found at 42º (2θ), which indicates the existence of a metallic copper (JCPDS: 04-0836) phase in Cu_2O-3 [20]. The result suggests that a high concentration of precursor favors the small quantity of Cu (0) in the sample. Besides phases, the crystallite size of samples was calculated based on Scherrer's equation based on (111) diffraction peak. It was found that the crystallite size of Cu_2O-1(1.77 nm) is smaller than the Cu_2O-2 (2.1 nm) and Cu_2O-3 (2.4 nm). Cu_2O-1 and Cu_2O-2 revealed the formation of nanoparticles (Fig. 2a, b). The nanoparticles were slightly agglomerated. However, Cu_2O-3 presented the octahedron morphology (Fig. 2c). The size of the octahedron consists of 0.5–1.5 µm. Furthermore, The FESEM elemental mapping and spectrum indicated the uniform distribution of Cu and O elements in the samples (Fig. S2).

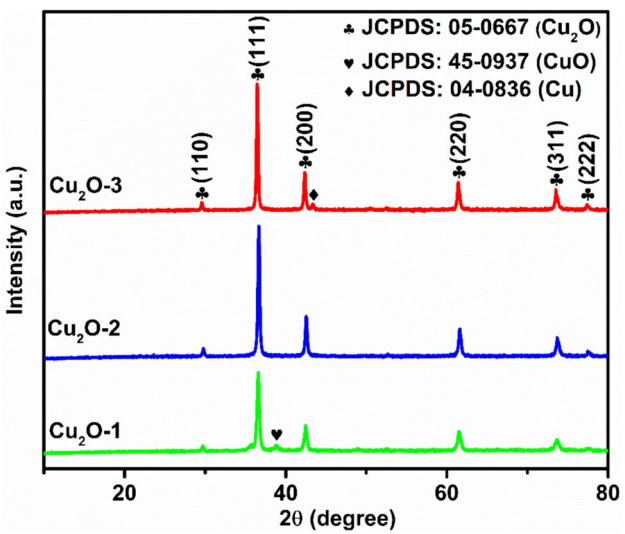

Figure 1 XRD patterns of samples.

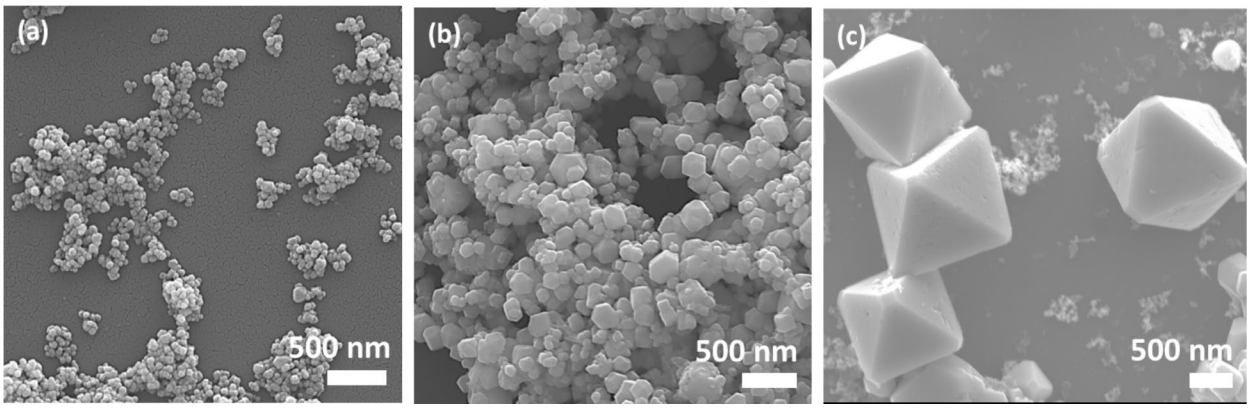

Figure 2 FESEM images of samples. **a** Cu_2O-1, **b** Cu_2O-2, and **c** Cu_2O-3. (Scale bar: 0.5 μm).

Figure 3 A schematic illustration of the formation mechanism of different sizes/morphologies of samples.

The mechanism related to the controlled synthesis of different morphologies/sizes was presented in Fig. 3. First, Cu_2O crystal nuclei were formed by the reaction between the salt solution of $Cu(NO_3)_2.3H_2O$ with $NaBH_4$ via the nucleation process. In the case of Cu_2O-1, the lower concentration of $Cu(NO_3)_2.3H_2O$ enhances the reduction rate that can generate multiple single nuclei. Also, the crystal nucleation rate is higher than the crystal's growth in Cu_2O-1. Due to this reason, a smaller size of nanoparticles was formed. However, the slight increase in precursor concentration lowers the reduction rate, and few nuclei may be produced in Cu_2O-2. In addition, these nuclei may collide with other nuclei to generate large size of particles [21]. Furthermore, at high concentrations, the precursor reduces the crystal nucleation rate than the crystal growth, which can increase the particle size in Cu_2O-3.

The detailed structural information of the Cu_2O-1 sample was shown by TEM, HRTEM, and high-angle annular dark-field scanning (HAADF) TEM images with elemental mapping (Fig. 4). The TEM images suggested the existence of nanoparticles in Cu_2O-1. The rough surface with several steps and kinks on the surface would provide a more active site for catalytic reaction. According to HRTEM image, the interplanar spacing of crystalline was found to be 0.246 nm, corresponding to Cu_2O (111) plane (Fig. 4b). The fringe spacing agreed with Cu_2O (JCPDS: 05–0667), revealing good agreement with XRD patterns (Fig. 1). The uniform distribution of copper and oxygen was observed in TEM imaging (Fig. 4c).

The chemical states and elemental composition of Cu_2O-1, Cu_2O-2, and Cu_2O-3 were measured via XPS spectra (Fig. 5). The Cu 2p spectra of samples were deconvoluted into $2p_{3/2}$ (Cu_2O-1: 935.79 eV, Cu_2O-2: 935.37 eV, and Cu_2O-3: 934.42 eV), $2p_{3/2}$ satellite (Cu_2O-1: 943.77 eV, Cu_2O-2: 943.80 eV, and Cu_2O-3: 943.60 eV), $2p_{1/2}$, (Cu_2O-1: 955.61 eV, Cu_2O-2: 955.42 eV, and Cu_2O-3: 954.12 eV), and $2p_{1/2}$ satellite (Cu_2O-1: 963.61 eV, Cu_2O-2: 963.66 eV, and Cu_2O-3: 962.74 eV). It suggests the existence of Cu^+ in samples (Fig. 5a–c) [22–24]. According to Fig. 5d–f, O 1s spectra demonstrated three distinct fitted peaks which were lattice oxygen (Cu_2O-1: 529.00 eV, Cu_2O-2: 528.81 eV, and Cu_2O-3: 529.17 eV), chemisorbed oxygen (Cu_2O-1:

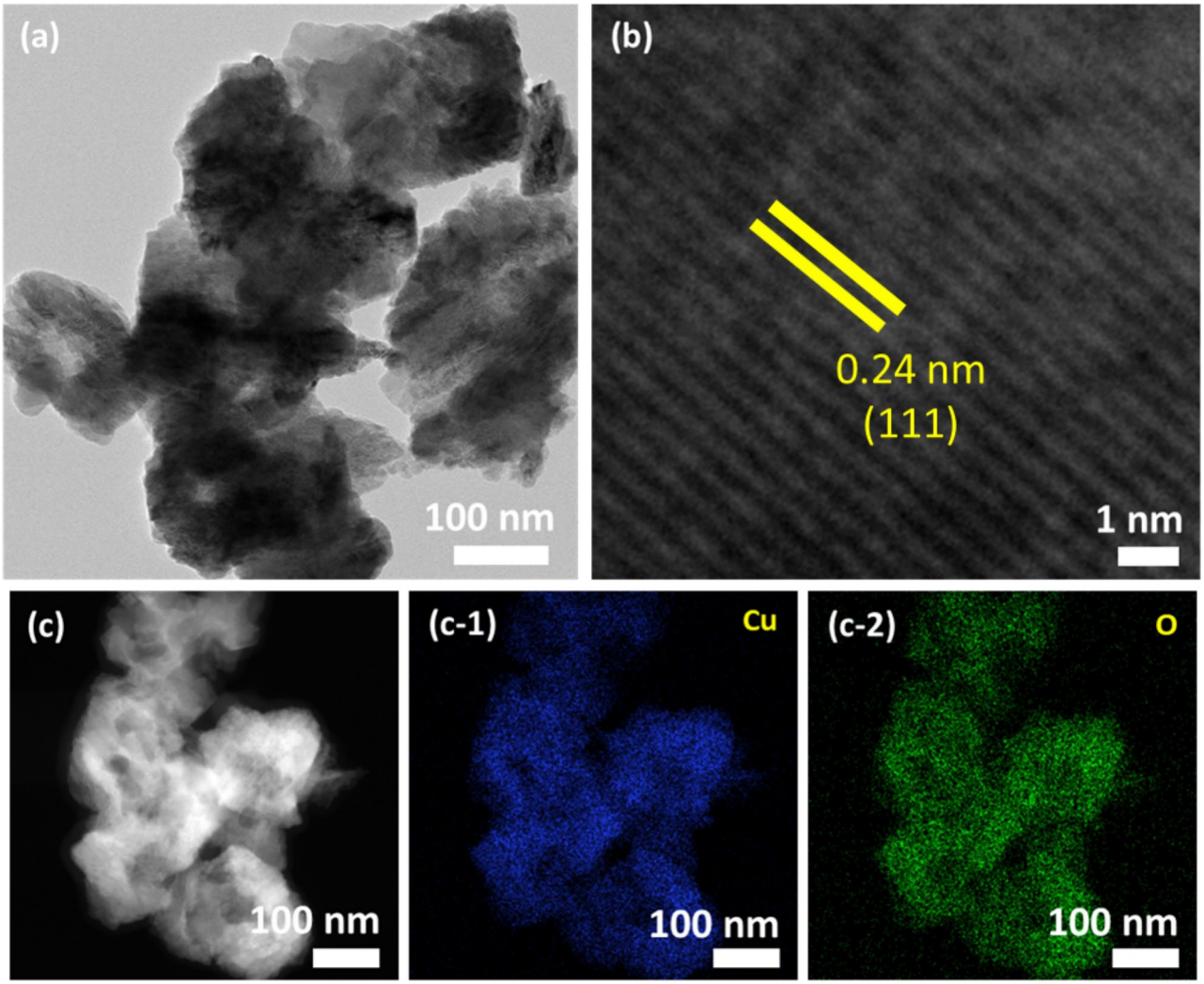

Figure 4 **a** TEM, **b** HRTEM and **c** HAADF-TEM images with EDX mapping of Cu_2O-1.

530.07 eV, Cu_2O-2: 530.41 eV, and Cu_2O-3: 530.96 eV), and oxygen vacancies (Cu_2O-1: 532.51 eV, Cu_2O-2: 532.04 eV, and Cu_2O-3: 532.61 eV) [25, 26]. This result also provides a higher oxygen vacancy in Cu_2O-1 nanoparticles. Furthermore, the survey spectra showed the presence of Cu and O in samples.

The electrochemical characterization of morphology controlled Cu_2O was performed by CV analysis that can determine the oxidation and reduction behavior of the electrocatalyst. Figure 6a–c represent the CV curves of Cu_2O-1, Cu_2O-2, and Cu_2O-3 in the potential range -0.6 to 0.6 V vs Ag/AgCl at the various scan rates (40 mV/s, 60 mV/s, 80 mV/s, and 100 mV/s), respectively. Each of the unsymmetrical CV profiles revealed the anodic (Cu_2O-1: 0.11 V, Cu_2O-2: 0.084 V, and Cu_2O-3: 0.089) and cathodic peaks (Cu_2O-1: −0.37 V, Cu_2O-2: −0.39 V, and Cu_2O-3: −0.37 V), indicating the redox reaction of Cu_2O. It can be attributed Cu(I)/Cu(II) redox reaction [18]. The oxidation and reduction peaks were shifted towards the positive and negative potential with increased scan rates, respectively. It may be associated with internal resistance over the electrode and charge diffusion polarization in the electrodes [27]. Also, the increase in scan rate promoted the current response, which suggests the kinetic of the interfacial oxidation and reduction reactions and the rapid rate of the ionic/electronic responses [28]. Moreover, Cu_2O-2 demonstrated lower current density than Cu_2O-1 and Cu_2O-3 (Figs. 6a–c, and S3). It indicates that nanoparticles and octahedron morphologies may

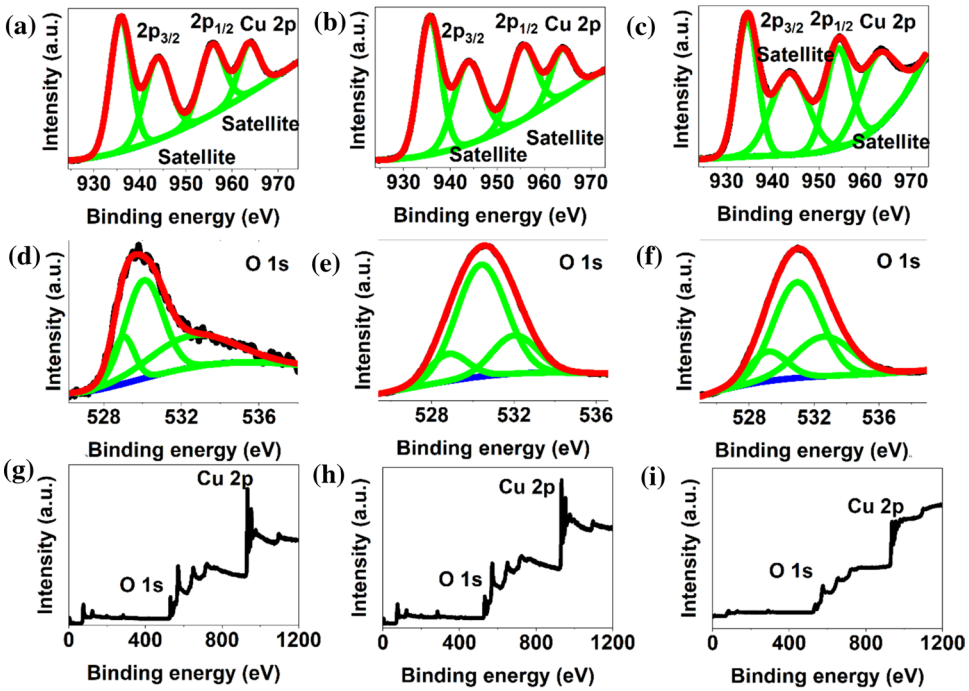

Figure 5 XPS analysis of Cu_2O-1 (**a** Cu 2p, **d** O1s, and **g** survey), Cu_2O-2 (**b** Cu 2p, **e** O1s, and **h** survey), and Cu_2O-3 (**c** Cu 2p, **f** O1s, and **i** survey).

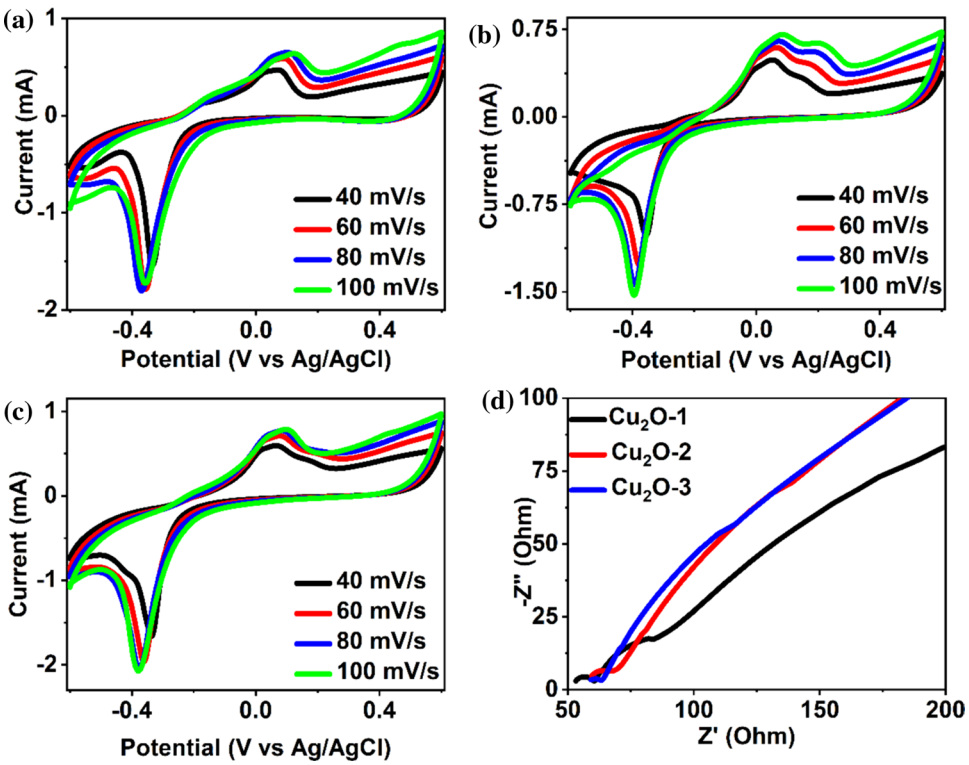

Figure 6 CV (**a** Cu_2O-1, **b** Cu_2O-2, and **c** a Cu_2O-3) and EIS plot of samples.

provide more active sites for electrocatalytic CO_2RR. The CV performance Cu-foil was evaluated to eliminate the interference from the substrate (Fig. S4). The current density of Cu-foil is observed to be lower than the Cu_2O samples. The electrochemical performance of catalysts was further explored by EIS measurements;

the results are presented in Fig. 6d. The catalysts have a semicircle and straight line in high-frequency and low-frequency regions. Compared to Cu_2O-2 and Cu_2O-1, Cu_2O-3 revealed a smaller semicircle diameter. In addition, an equivalent circuit model is shown in Fig. S5. The estimated value of solution resistance, charge transfer resistance, Warburg coefficient, and electric double-layer capacitance are shown in Table S1. The results suggest that Cu_2O-1 and Cu_2O-3 demonstrated lower charge transfer resistance than Cu_2O-2. It suggests the smaller charge-transfer resistance in nanoparticles and octahedrons. The superior charge transfer efficiency and good conductivity of these catalysts can enhance the electrocatalytic CO_2RR.

To better elucidate the effect of Cu_2O morphologies on the electrocatalytic CO_2RR performance, LSV tests were performed for the Cu_2O-1, Cu_2O-2, and Cu_2O-3 catalysts at a sweep rate of 20 mV/s in CO_2-saturated 0.5 M $KHCO_3$ (Fig. 7a). As observed, Cu_2O-1 exhibited higher current densities and lowest onset potential than Cu_2O-2, and Cu_2O-3 catalysts. The possible reason may be associated with good electrical conductivity that can accelerate the transfer of electrons during the electrocatalytic CO_2RR. Also, Cu_2O-1 has the smallest current at a voltage of −0.25 V versus RHE. The possible reason may relate to variation in the electrochemical reaction rate [29]. To investigate the reason for the greater CO_2RR performance of the Cu_2O-1 electrode than others, Tafel slopes were evaluated (Fig. 7b). The Tafel slopes of the Cu_2O-1, Cu_2O-2, and Cu_2O-3 catalysts revealed 94.62, 117.81, and 101.83 mV/dec, respectively. It suggests that Cu_2O-1 exhibited the lowest Tafel slope. These results also indicate that the surface of Cu_2O-1 nanoparticles makes the electrocatalytic CO_2RR easier than others by enhancing the initial transfer rate of electrons to the CO_2 molecules.

CO_2 electroreduction using three catalysts was conducted in a 0.5 M $KHCO_3$ under applied cathode potential to investigate the catalytic activities towards the product distribution. The chronoamperometry measurements of Cu_2O samples at −0.3 V versus RHE for 400 s were shown in Fig. S6. It indicates that Cu_2O-1 nanoparticles revealed higher current density than others. In addition, the Cu-foil showed lower current density than other Cu_2O samples (Fig. S7). The calculation of FEs was provided in supplementary information and Table S2. FEs of CO (Cu_2O-1: 11.90%, Cu_2O-2: 9.76%, and Cu_2O-3: 12.1%), CH_4 (Cu_2O-1: 76.61%, Cu_2O-2: 65.11%, and Cu_2O-3: 74.63%), and C_2H_6 (Cu_2O-1: 1.87%, Cu_2O-2: 2.39%, and 2.60%) were obtained during electrocatalytic CO_2RR samples (Fig. 7c). These results suggested that CH_4 and CO/C_2H_6 were major and minor products, respectively.

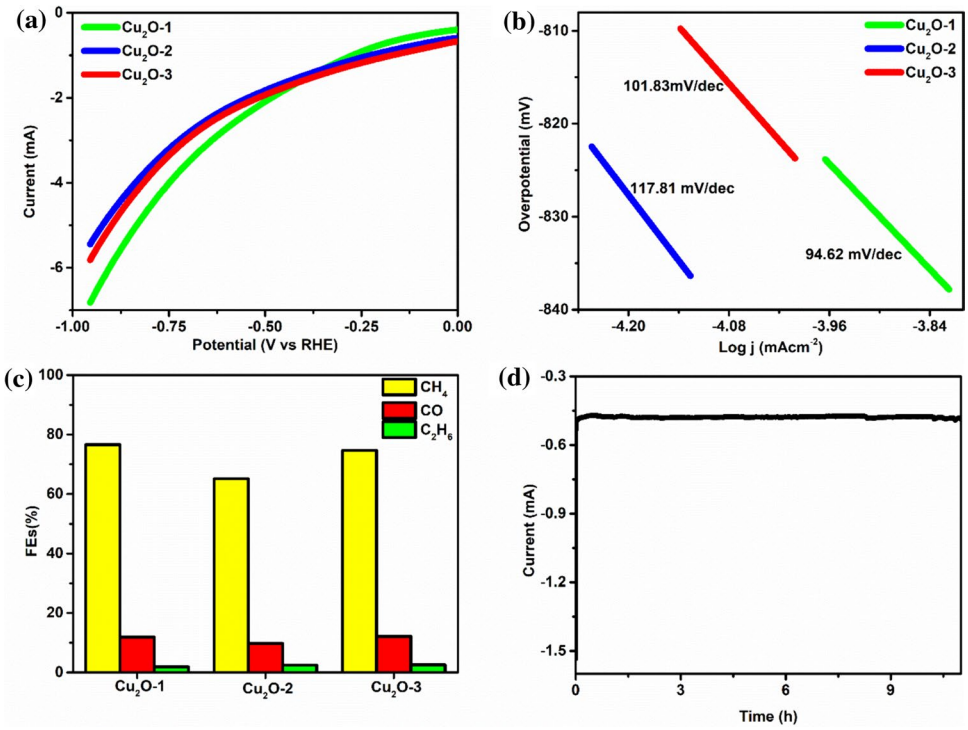

Figure 7 **a** LSV, **b** Tafel slope, **c** FEs of the electrodes, and **d** stability test of Cu_2O-1 for CO_2 reduction over 11 h.

Based on the hydrocarbon products, the possible mechanisms have been proposed. At first, the CO_2 molecules are adsorbed and activated on the crystalline plane of Cu_2O (111). Then, it is quickly converted into *COOH via multiple proton-coupled electron transfer (PCET) processes. In addition, this process coupled with *COOH intermediate to produce *CO. In addition, Cu_2O (111) tends to provide stable adsorption of *CO. The adsorption of *CO shows superior stability on the catalyst surface, making C1 and C2 products possible. The desorption of *CO from the active site to form CO [30, 31]. Furthermore, *CO may convert into *CHO, *CH_2O and *CH_3O intermediates via PCET to generate CH_4. Also, *CHO is converted into *CH_3 via *CH_2 formation by PCET. Then, dimerization of CH_3 produces the C_2H_6 [9, 32, 33].

The high selectivity of Cu_2O for CH_4 may be attributed to (111) crystalline plane that can provide active sites. Also, abundant hydroxyl groups tend to tune the stability of intermediates for CH_4 formation by hydrogen bonds [23]. The low selectivity of C_2H_6 may relate to the kinetic barrier for the coupling, which can effectively influence the degree of the adsorbed CO hydrogenation. Such type of kinetic barrier decreases with an increase in the degree of the surface-bound CO hydrogenation that may favor C_2H_6 [34]. Also, the adsorbed CO is an intermediate state of C1 and C2 products. Due to this reason, low selectivity of Cu_2O for CO was observed [35]. Cu_2O-1 demonstrated higher electrocatalytic CO_2RR efficiency compared to others. It consists of nanosized among all samples. It consists of more active sites, oxygen vacancy, high flexibility, and rapid oxygen diffusion along the dense boundary between the nanoparticles [35]. Also, the co-existence of Cu^+ and Cu^{2+} ions can provide active sites and more favorable free energy for the production of *CO intermediates that facilitate the generation of C–C bonds for C_{2+} formation [36]. Besides producing CO, CH_4, and C_2H_6, stability is important for electrocatalysts towards CO_2RR efficiencies. According to the stability test of Cu_2O-1, there was no decay of current densities over an 11 h period, indicating significant stability (Fig. 7d). Furthermore, the stability of the catalyst was investigated using XRD and FESEM analyses. Figure S8 presented the XRD patterns of Cu_2O-1 after electrocatalytic stability after 11 h. It was observed that the XRD of the used catalyst is well matched with the fresh catalyst. In addition, the

Table 1 Comparison of the catalytic performance of synthesized Cu_2O with other Cu_2O-based catalysts

Catalyst	Synthesis method	Electrolyte	FEs (%)	E versus RHE (V)	Stability (h)	References
S-Cu_2O	Hydrothermal	0.1 M $KHCO_3$	HCOO- (66.1%)	− 1.0	2	[37]
Cu_2O/ZnO	Solvothermal	0.1 M $KHCO_3$	CO (65.7%) and H_2	− 0.6 to − 1.4	2	[38]
Cu@Cu_2O	Solvothermal	0.1 M $KHCO_3$	C_2H_4 (44%)	− 1.08	6	[39]
Ag–Cu/Cu_2O	Ultrasonic synthetic	1 M KOH	C_2H_5OH (19.2%)	–	8	[40]
MOF- Cu@Cu_2O	Hydrothermal	0.5 M $KHCO_3$	CH_3OH (45%)	− 0.7	10	[41]
Cu-Cu_2O/LDH	Electrochemical reduction	0.1 M $HClO_4$	C_2H_4 (36%)	− 1.1	20	[42]
Cu-Cu_2O	Electrodeposition	0.1 M $KHCO_3$	C_2H_4 (51%)	− 0.76	10	[43]
Cu_2O	Interface-induce	0.1 M $KHCO_3$	C_2H_4 (31.1%)	− 1.15 V	1.6 h	[44]
Cu_2O	Chemical reduction and deposition	0.5 M NaOH	CH_3OH	− 1.7 V	4 h	[45]
Cu_2O/CuO	electrodeposition	0.5 M $KHCO_3$, 10 mM pyridine, and HCl	CH_3OH (6.46%)	− 1.3 V	2 h	[24]
Cu_2O@Au	Galvanic replacement reaction	0.1 M $KHCO_3$	CO (30.1%)	− 1.0 V	–	[46]
Cu_2O/Cu-$PdCl_3$	Electrodeposition	0.1 M $KHCO_3$	C_2H_6 (30.1%)	− 1.0 V	1.5 h	[47]
ZnO@Cu_2O	Epitaxial growth	0.1 M $KHCO_3$	C_2H_4 (33.5%) and C_2H_5OH (16.3%)	− 1.0 V	–	[48]
Cu_2O/CuS	Hydrothermal	0.1 M $KHCO_3$	$HCOO^-$ (67.6%)	− 0.9 V	3 h	[49]
Cu_2O	Chemical reduction	0.5 M $KHCO_3$	CO (11.9%), CH_4, (76.61%), and C_2H_6 (1.87%)	− 0.3 V	11 h	Our work

FESEM image of the used catalyst was like that of the unused catalyst (Fig. S9). These characterization techniques suggest the excellent stability of the catalyst for electrocatalytic CO_2RR. Table 1 shows a comparison of Cu_2O with previously reported Cu_2O-based electrode materials. Our results are comparable to those of previous literature.

Conclusion

In summary, various morphologies/sizes of Cu_2O were synthesized by the chemical reduction method at low temperatures by changing the concentration of metal ions. XRD suggested the trace amount of CuO and Cu phases at low and high concentrations of precursors, respectively, in the Cu_2O catalyst. FESEM provided evidence of different sizes/morphologies. Elemental mapping demonstrated the uniform distribution of Cu and O in samples. The evidence of the Cu_2O (111) plane was proved by the HRTEM image. The electrochemical characterization (CV, EIS, LSV, Tafel plot, and chronoamperometry curves) was carried out for electrochemical CO2RR performance on H-type cells. Cu_2O nanoparticles revealed higher electrocatalytic CO_2RR efficacy than others (bigger particles and octahedron). In addition, Cu_2O catalysts tend to provide CH_4 (major) and minor (CO and C_2H_6) products at −0.3 V versus RHE. The possible reasons for the enhancement of electrocatalytic efficiency of Cu_2O nanoparticles are the presence of a greater number of active sites, oxygen vacancy, good electrical conductivity, the ability of rapid electron transfer, and a trace amount of Cu^{2+} phase. In conclusion, tuning Cu_2O morphology using low temperature chemical reduction method is a great way to make efficient catalysts for generating CO, CH_4, and C_2H_6 via electrocatalytically CO_2RR.

Acknowledgements

The National Science Foundation the Excellence in Research Award (2100710) USA supported this research. Some of the characterizations were performed in Joint School of Nanoscience and Nanoengineering, a member of the Southeastern Nanotechnology Infrastructure Corridor and National Nanotechnology Coordinated Infrastructure, which is supported by the National Science Foundation (Grant ECCS-1542174).

Funding

Open access funding provided by the Carolinas Consortium. National Science Foundation, 2100710, Bishnu Bastakoti

Data availability

The data supporting this study's findings are available from the corresponding author upon reasonable request.

Declarations

Conflict of interest The authors declare that they have no known competing financial interests or personal relationships that could have appeared to influence the work reported in this paper.

Supplementary Information The online version contains supplementary material available at https://doi.org/10.1007/s10853-024-10004-z.

References

[1] Wu J, Huang Y, Ye W, Li Y (2017) CO_2 reduction: from the electrochemical to photochemical approach. Adv Sci 4:1–29. https://doi.org/10.1002/advs.201700194

[2] Cai J, Li D, Jiang L et al (2023) Review on CeO_2-based photocatalysts for photocatalytic reduction of CO_2: progresses and perspectives. Energy Fuels 37:4878–4897. https://doi.org/10.1021/acs.energyfuels.3c00120

[3] KC BR, Kumar D, Bastakoti BP (2024) Block copolymer-mediated synthesis of TiO_2/RuO_2 nanocomposite for efficient oxygen evolution reaction. J Mater Sci 59:10193–10206. https://doi.org/10.1007/s10853-024-09702-5

[4] Ray SK, Kokayi M, Desai R et al (2024) Ni/NiO nanoparticles loaded carbon sphere for high-performance supercapacitor. Mater Chem Phys 320:129403. https://doi.org/10.1016/j.matchemphys.2024.129403

[5] Ray SK, Bastakoti BP (2024) Improved supercapacitor and oxygen evolution reaction performances of morphology-controlled cobalt molybdate. Int J Hydrogen Energy 51:1109–1118. https://doi.org/10.1016/j.ijhydene.2023.11.003

[6] Ray SK, Dahal R, Ashie MD et al (2024) Nanosheet assembled microspheres metal (Zn, Ni, and Cu) indium sulfides for highly selective CO_2 electroreduction to methane. Catal Sci Technol. https://doi.org/10.1039/D4CY00270A

[7] Liang S, Altaf N, Huang L et al (2020) Electrolytic cell design for electrochemical CO_2 reduction. J CO_2 Util 35:90–105. https://doi.org/10.1016/j.jcou.2019.09.007

[8] Ma W, He X, Wang W et al (2021) Electrocatalytic reduction of CO_2 and CO to multi-carbon compounds over Cu-based catalysts. Chem Soc Rev 50:12897–12914. https://doi.org/10.1039/d1cs00535a

[9] Woldu AR, Huang Z, Zhao P et al (2022) Electrochemical CO_2 reduction (CO_2RR) to multi-carbon products over copper-based catalysts. Coord Chem Rev 454:214340. https://doi.org/10.1016/j.ccr.2021.214340

[10] Kibria MG, Edwards JP, Gabardo CM et al (2019) Electrochemical CO_2 reduction into chemical feedstocks: from mechanistic electrocatalysis models to system design. Adv Mater 31:1–24. https://doi.org/10.1002/adma.201807166

[11] Arán-Ais RM, Rizo R, Grosse P et al (2020) Imaging electrochemically synthesized Cu_2O cubes and their morphological evolution under conditions relevant to CO_2 electroreduction. Nat Commun 11:1–8. https://doi.org/10.1038/s41467-020-17220-6

[12] Munkaila S, Dahal R, Kokayi M et al (2022) Hollow structured transition metal phosphates and their applications. Chem Rec. 22: e20220084. https://doi.org/10.1002/tcr.202200084

[13] Wei H, Huang K, Zhang L et al (2018) Ice melting to release reactants in solution syntheses. Angew Chemie Int Ed 57:3354–3359. https://doi.org/10.1002/anie.201711128

[14] Ray SK, Dahal R, Ashie MD, Bastakoti BP (2024) Decoration of Ag nanoparticles on $CoMoO_4$ rods for efficient electrochemical reduction of CO_2. Sci Rep 14:1–10. https://doi.org/10.1038/s41598-024-51680-w

[15] Chen CS, Handoko AD, Wan JH et al (2015) Stable and selective electrochemical reduction of carbon dioxide to ethylene on copper mesocrystals. Catal Sci Technol 5:161–168. https://doi.org/10.1039/c4cy00906a

[16] Zhang M, Chen Z, Wang Y et al (2019) Enhanced light harvesting and electron-hole separation for efficient photocatalytic hydrogen evolution over Cu_7S_4-enwrapped Cu_2O nanocubes. Appl Catal B Environ 246:202–210. https://doi.org/10.1016/j.apcatb.2019.01.042

[17] Wang S, Kou T, Baker SE et al (2020) Recent progress in electrochemical reduction of CO_2 by oxide-derived copper catalysts. Mater Today Nano 12:100096. https://doi.org/10.1016/j.mtnano.2020.100096

[18] Pawar SM, Kim J, Inamdar AI et al (2016) Multi-functional reactively-sputtered copper oxide electrodes for supercapacitor and electro-catalyst in direct methanol fuel cell applications. Sci Rep 6:1–9. https://doi.org/10.1038/srep21310

[19] Mallik M, Monia S, Gupta M et al (2020) Synthesis and characterization of Cu_2O nanoparticles. J Alloys Compd 829:154623. https://doi.org/10.1016/j.jallcom.2020.154623

[20] Yang L, Su J (2021) Controllable fabrication and self-assembly of Cu nanostructures: the role of Cu2+complexes. RSC Adv 11:17715–17720. https://doi.org/10.1039/d1ra02408f

[21] Ebrahimzadeh F, Fung KZ (2016) One-pot synthesis of size and shape controlled copper nanostructures in aqueous media and their application for fast catalytic degradation of organic dyes. J Chem Res 40:552–557. https://doi.org/10.3184/174751916X14718784323425

[22] Li X, Kong W, Qin X et al (2020) Self-powered cathodic photoelectrochemical aptasensor based on in situ–synthesized CuO-Cu_2O nanowire array for detecting prostate-specific antigen. Microchim Acta 187:325 https://doi.org/10.1007/s00604-020-04277-9

[23] Yi J, Xie R, Xie Z et al (2020) Highly selective CO_2 electroreduction to CH_4 by in situ generated Cu_2O single-type sites on a conductive MOF: stabilizing key intermediates with hydrogen bonding. Angew Chemie 132:23849–23856. https://doi.org/10.1002/ange.202010601

[24] Roy A, Jadhav HS, Gil Seo J (2021) Cu_2O/CuO electrocatalyst for electrochemical reduction of carbon dioxide to

methanol. Electroanalysis 33:705–712. https://doi.org/10.1002/elan.202060265

[25] Zhang YH, Cai XL, Guo DY et al (2019) Oxygen vacancies in concave cubes Cu_2O-reduced graphene oxide heterojunction with enhanced photocatalytic H_2 production. J Mater Sci Mater Electron 30:7182–7193. https://doi.org/10.1007/s10854-019-01036-2

[26] Wang Y, Lü Y, Zhan W et al (2015) Synthesis of porous Cu_2O/CuO cages using Cu-based metal-organic frameworks as templates and their gas-sensing properties. J Mater Chem A 3:12796–12803. https://doi.org/10.1039/c5ta01108f

[27] Aljaafari A, Parveen N, Ahmad F et al (2019) Self-assembled cube-like copper oxide derived from a metal-organic framework as a high-performance electrochemical supercapacitive electrode material. Sci Rep 9:1–11. https://doi.org/10.1038/s41598-019-45557-6

[28] Zhang F, Yuan C, Zhu J et al (2013) Flexible films derived from electrospun carbon nanofibers incorporated with Co_3O_4 hollow nanoparticles as self-supported electrodes for electrochemical capacitors. Adv Funct Mater 23:3909–3915. https://doi.org/10.1002/adfm.201203844

[29] Fu W, Liu Z, Wang T et al (2020) ACS Sustain Chem Eng 8:15223–15229. https://doi.org/10.1021/acssuschemeng.0c04873

[30] Lee S, Kim D, Lee J (2015) Electrocatalytic production of C3–C4 compounds by conversion of CO_2 on a chloride-induced bi-phasic Cu_2O-Cu catalyst. Angew Chemie 127:14914–14918. https://doi.org/10.1002/ange.201505730

[31] Zhang L, Zhao ZJ, Gong J (2017) Nanostructured materials for heterogeneous electrocatalytic CO_2 reduction and their related reaction mechanisms. Angew Chemie Int Ed 56:11326–11353. https://doi.org/10.1002/anie.201612214

[32] Handoko AD, Chan KW, Yeo BS (2017) $-CH_3$ mediated pathway for the electroreduction of CO_2 to ethane and ethanol on thick oxide-derived copper catalysts at low overpotentials. ACS Energy Lett 2:2103–2109. https://doi.org/10.1021/acsenergylett.7b00514

[33] Ren D, Deng Y, Handoko AD et al (2015) Selective electrochemical reduction of carbon dioxide to ethylene and ethanol on copper(I) oxide catalysts. ACS Catal 5:2814–2821. https://doi.org/10.1021/cs502128q

[34] Kas R, Kortlever R, Milbrat A et al (2014) Electrochemical CO_2 reduction on Cu_2O-derived copper nanoparticles: controlling the catalytic selectivity of hydrocarbons. Phys Chem Chem Phys 16:12194–12201. https://doi.org/10.1039/c4cp01520g

[35] Jung H, Lee SY, Lee CW et al (2019) Electrochemical fragmentation of Cu_2O nanoparticles enhancing selective C-C coupling from CO_2 reduction reaction. J Am Chem Soc 141:4624–4633. https://doi.org/10.1021/jacs.8b11237

[36] Liu Y, Liu H, Wang C et al (2023) Reconstructed Cu/Cu_2O(I) catalyst for selective electroreduction of CO_2 to C2+ products. Electrochem Commun 150:107474. https://doi.org/10.1016/j.elecom.2023.107474

[37] Yuan H, Liu Z, Sang S, Wang X (2023) Dynamic re-construction of sulfur tailored Cu_2O for efficient electrochemical CO_2 reduction to formate over a wide potential window. Appl Surf Sci 613:156130. https://doi.org/10.1016/j.apsusc.2022.156130

[38] Azenha C, Mateos-Pedrero C, Lagarteira T, Mendes AM (2023) Tuning the selectivity of Cu_2O/ZnO catalyst for CO_2 electrochemical reduction. J CO_2 Util 68: 102368. https://doi.org/10.1016/j.jcou.2022.102368

[39] Ye M, Shao T, Liu J et al (2023) Phase engineering of Cu@Cu_2O core-shell nanospheres for boosting tandem electrochemical CO_2 reduction to C2+ products. Appl Surf Sci 622:156981. https://doi.org/10.1016/j.apsusc.2023.156981

[40] Su W, Ma L, Cheng Q et al (2021) Highly dispersive trace silver decorated Cu/Cu2O composites boosting electrochemical CO_2 reduction to ethanol. J CO_2 Util 52:101698. https://doi.org/10.1016/j.jcou.2021.101698

[41] Yang X, Cheng J, Yang X et al (2022) MOF-derived Cu@Cu_2O heterogeneous electrocatalyst with moderate intermediates adsorption for highly selective reduction of CO_2 to methanol. Chem Eng J 431:134171. https://doi.org/10.1016/j.cej.2021.134171

[42] Altaf N, Liang S, Huang L, Wang Q (2020) Electro-derived Cu-Cu_2O nanocluster from LDH for stable and selective C2 hydrocarbons production from CO_2 electrochemical reduction. J Energy Chem 48:169–180. https://doi.org/10.1016/j.jechem.2019.12.013

[43] Ren X, Zhang X, Cao X, Wang Q (2020) Efficient electrochemical reduction of carbon dioxide into ethylene boosted by copper vacancies on stepped cuprous oxide. J CO_2 Util 38:125–131. https://doi.org/10.1016/j.jcou.2020.01.018

[44] Wang W, Ning H, Yang Z et al (2019) Interface-induced controllable synthesis of Cu_2O nanocubes for electroreduction CO_2 to C_2H_4. Electrochim Acta 306:360–365. https://doi.org/10.1016/j.electacta.2019.03.146

[45] Chang T-Y, Liang R-M, Wu P-W et al (2009) Electrochemical reduction of CO_2 by Cu_2O-catalyzed carbon clothes. Mater Lett 63:1001–1003. https://doi.org/10.1016/j.matlet.2009.01.067

[46] Tan W, Cao B, Xiao W et al (2019) Electrochemical reduction of CO_2 on hollow cubic Cu_2O@Au nanocomposites. Nanoscale Res Lett 14:2–8. https://doi.org/10.1186/s11671-019-2892-3

[47] Chen CS, Wan JH, Yeo BS (2015) Electrochemical reduction of carbon dioxide to ethane using nanostructured Cu_2O-derived copper catalyst and palladium(II) chloride. J Phys Chem C 119:26875–26882. https://doi.org/10.1021/acs.jpcc.5b09144

[48] Zhu S, Ren X, Li X et al (2021) Core-shell ZnO@Cu_2O as catalyst to enhance the electrochemical reduction of carbon dioxide to C2 products. Catalysts. https://doi.org/10.3390/catal11050535

[49] Wang S, Kou T, Varley JB et al (2021) Cu_2O/CuS nanocomposites show excellent selectivity and stability for formate generation via electrochemical reduction of carbon dioxide. ACS Mater Lett 3:100–109. https://doi.org/10.1021/acsmaterialslett.0c00520